Origami-Based Reconfigurable Metamaterials for Tunable Chirality

Zuojia Wang, Liqiao Jing, Kan Yao, Yihao Yang, Bin Zheng, Costas M. Soukoulis, Hongsheng Chen, and Yongmin Liu**

Origami is the art of folding two-dimensional (2D) materials, such as a flat sheet of paper, into complex and elaborate three-dimensional (3D) objects. This study reports origami-based metamaterials whose electromagnetic responses are dynamically controllable via switching the folding state of Miura-ori split-ring resonators. The deformation of the Miura-ori unit along the third dimension induces net electric and magnetic dipoles of split-ring resonators parallel or anti-parallel to each other, leading to the strong chiral responses. Circular dichroism as high as 0.6 is experimentally observed while the chirality switching is realized by controlling the deformation direction and kinematics. In addition, the relative density of the origami metamaterials can be dramatically reduced to only 2% of that of the unfolded structure. These results open a new avenue toward lightweight, reconfigurable, and deployable metadevices with simultaneously customized electromagnetic and mechanical properties.

Over the past decade, metamaterials have become an important research area due to their exotic material properties, which are primarily determined by the physical structures of the subwavelength building blocks rather than the chemical constitutions that the metamaterials are made of.[1,2] The transformative concept of metamaterials has enabled many novel electromagnetic and optical properties and applications, ranging from negative refractive indices[3,4] and giant chirality[5] to superlens,[6] invisibility cloaking,[7] and wireless energy transfer.[8] Very recently, metasurfaces, the two-dimensional (2D) counterpart of metamaterials, provide an alternative scheme to steer the flow of electromagnetic waves by arranging artificial structures on a flat interface to engineer the phase profile, polarization, and trajectory of electromagnetic waves.[9–12] Compared with three-dimensional (3D) metamaterials, planar metasurfaces exhibit relatively low loss and deep subwavelength thickness, and therefore they are highly suitable for on-chip integration.[13,14] However, structural modification is generally very challenging once metamaterials and metasurfaces are fabricated, rendering them nonreconfigurable.

Substantial efforts have been devoted to achieve the dynamical control over the functionalities of electromagnetic and optical devices,[15] by means of external stimuli including heat,[16,17] mechanic stretching,[18] electrostatic and magnetic forces,[19–21] and gas pressure.[22] Phase-change materials, whose complex refractive indices are different between their amorphous and crystalline states, have also been applied to realize reconfigurable devices.[23,24] All these approaches can be generally categorized into two groups: modulating the optical parameters of materials or changing the structural shapes. For the latter strategy, the shape-changing capability over three dimensions is extremely important for metamaterial structures, because some optical phenomena, such as the intrinsic chiroptical effect, can only exist in 3D structures. In particular, the continuous transformation among arbitrary shapes promises an unprecedented opportunity for ultrawide dynamical tuning range in reconfigurable metadevices.

One very promising technique to implementing reconfigurable metamaterials is origami, the ancient art of folding a sheet of paper into complex and elaborate 3D objects. Origami exists in a variety of nature systems such as insect wings,[25] leaves,[26] and embryonic intestines.[27,28] In recent years, origami has attracted significant interest of scientists and engineers because of its ability of creating various shape-changing materials.[29,30] This design principle has stimulated many applications, ranging from solar arrays,[31] deformable electronics,[32] and self-folding machines[33] to mechanical metamaterials.[34–37] Among

Prof. Z. Wang, Prof. Y. Liu
Department of Mechanical and Industrial Engineering
Northeastern University
Boston, MA 02115, USA
E-mail: y.liu@northeastern.edu

Prof. Z. Wang, L. Jing, Y. Yang, Dr. B. Zheng, Prof. H. Chen
State Key Laboratory of Modern Optical Instrumentation
Zhejiang University
Hangzhou 310027, China
E-mail: hansomchen@zju.edu.cn

Prof. Z. Wang
School of Information Science and Engineering
Shandong University
Jinan 250100, China

K. Yao, Prof. Y. Liu
Department of Electrical and Computer Engineering
Northeastern University
Boston, MA 02115, USA

Y. Yang, Prof. C. M. Soukoulis
Department of Physics and Astronomy and Ames Laboratory-U.S. DOE
Iowa State University
Ames, IA 50011, USA

Prof. C. M. Soukoulis
Institute of Electronic Structure and Laser
FORTH 71110, Heraklion, Crete, Greece

DOI: 10.1002/adma.201700412

different classes of origami patterns, Miura-ori is a special case of rigid origami in which rigid panels (facets) are connected through perfect hinges, leading to dynamically and continuously alterable shapes. The structure mechanics of Miura-ori tessellated fold pattern are dominated by the kinematics of the folding, which only depends on the geometry and therefore is scale-independent.[34] Study on deformation kinematics shows that the in-plane and out-of-plane Poisson's ratios of a Miura-ori structure are equal in magnitude but opposite in signs.[35] Bistability and multistability in the origami patterns have been used to create functional materials with alterable compressive modulus.[36–38] In addition, low relative density with preserved folding kinematics can be achieved by stacking individual Miura-ori sheets together,[34] while increased stiffness with only one deformation mode is realized in assembly of origami tube structures.[39] The richness of mathematics in origami, together with its unique mechanical features, provides a versatile platform to create origami-based deployable and reconfigurable devices. However, the research of tailoring other material properties by the concept of origami is still in infancy.

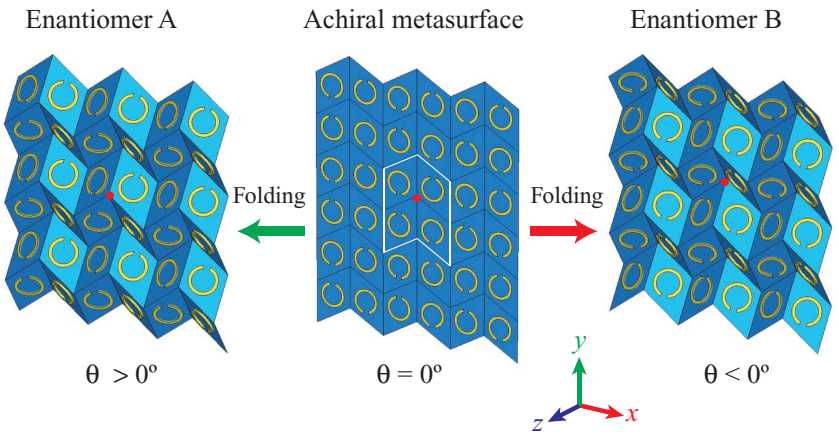

Figure 1. Schematic of the construction of Miura-ori chiral metamaterials. Split-ring resonators are periodically arranged to form an achiral metasurface (middle panel). One Miura-ori unit cell (outlined by the white lines) consists of four split-ring resonators located at the centers of four identical parallelograms. The 2D metasurface can be continuously transformed into 3D chiral metamaterials, that is, enantiomer A (left panel) and B (right panel), following the folding principle of Miura-ori patterns. The chirality switching is achieved by changing the deformation direction of the planar metasurface.

Here, we propose and demonstrate an origami-based reconfigurable metamaterial, whose electromagnetic response can be switched between nonchiral and chiral states at dual-band wavelengths. Split-ring resonators[40,41] are printed on rigid Miura-ori patterns to realize periodically arranged meta-atoms, and the control over the handedness of the structure is achieved by the Miura-ori deformation. Numerical and experimental results show that the resonant modes exhibit gradually enhanced chiroptical responses when transforming the 2D metasurface into 3D origami metamaterials. The underlying mechanism is the breaking of mirror symmetry of the folded 3D origami metamaterials, which is confirmed by detailed analyses of the excited electrical and magnetic dipoles and their relative orientations. Circular dichroism (CD) as high as 0.6 is experimentally observed while the chirality switching is realized by controlling the deformation direction and kinematics. Furthermore, the relative density of the 3D Miura-ori metamaterial is reduced to as small as 2% of that of the unfolded planar metasurface, thus providing a very promising method to construct lightweight reconfigurable metamaterials.

The concept of origami-based reconfigurable metamaterial is shown in **Figure 1**. First, split-ring resonators, one of the widely studied metamaterial structures, are printed on a flat sheet to construct an achiral metasurface. The achiral feature originates from the mirror symmetry with respect to the *xy*- and *xz* -planes. Next, the 2D metasurface is transformed into 3D geometries following the folding principle of the Miura-ori pattern.[34] The Miura-ori unit in our design is composed of four identical parallelograms that are connected by convex mountain and concave valley creases (i.e., the folding lines). Vertices are formed when four creases intersect and each parallelogram is preserved as a rigid facet in the folding process. In order to break the mirror symmetry of the Miura-ori pattern for the purpose of strong chirality, two neighboring split-ring resonators are orientated along the opposite directions. It is noticeable that such Miura-ori metasurface can be folded into two kinds of chiral enantiomers, labeled as A and B, which are mirror images of each other about the *yz*-plane. The folding angle θ is defined as the dihedral angle between the folded facets and the *xy*-plane (more details can be found in the Supporting Information). A positive (negative) sign of θ corresponds to the motion of the center vertex (the red spot in Figure 1) of each unit cell toward the + *z* (–*z*) direction. In this context, we assume the Miura-ori pattern is folded from an ideal material with infinite stretching modulus and therefore it has only one degree of freedom described by the folding angle θ.

A proof-of-principle origami metamaterial is designed in the microwave region with the geometric parameters illustrated in **Figure 2**a. For simplicity, each parallelogram has the same edge length of $a = b = 10$ mm and a vertex angle of $\gamma = 60°$. Four split-ring resonators are located at the centers of the parallelograms with identical dimensions yet different orientations. The inner and outer radii of each split-ring are $r_1 = 3$ mm and $r_2 = 3.5$ mm, respectively, while the gap size is $g = 1$ mm. The solid (dashed) lines correspond to the mountain (valley) creases of enantiomer A (B). This unfolded metasurface has mirror symmetries about both the *xy*- and *xz*-planes, and hence does not exhibit intrinsic chirality, although extrinsic chirality can be achieved from 2D structures subjected to oblique illumination.[42,43] Since the gaps of split-ring resonators are all oriented along the + *y* or – *y* directions, the 2D metasurface exhibits anisotropic responses. The electromagnetic response of a planar metasurface can be described by Jones matrix $T_{\text{circ}} = \begin{pmatrix} t_{\text{RR}} & t_{\text{RL}} \\ t_{\text{LR}} & t_{\text{LL}} \end{pmatrix}$. Here, t_{RR} and t_{LR} are the co- and cross-polarized transmission coefficients with the incidence of right-handed circularly polarized (RCP) waves, respectively, while t_{LL} and t_{RL} are the counterparts for left-handed circularly polarized (LCP) waves.

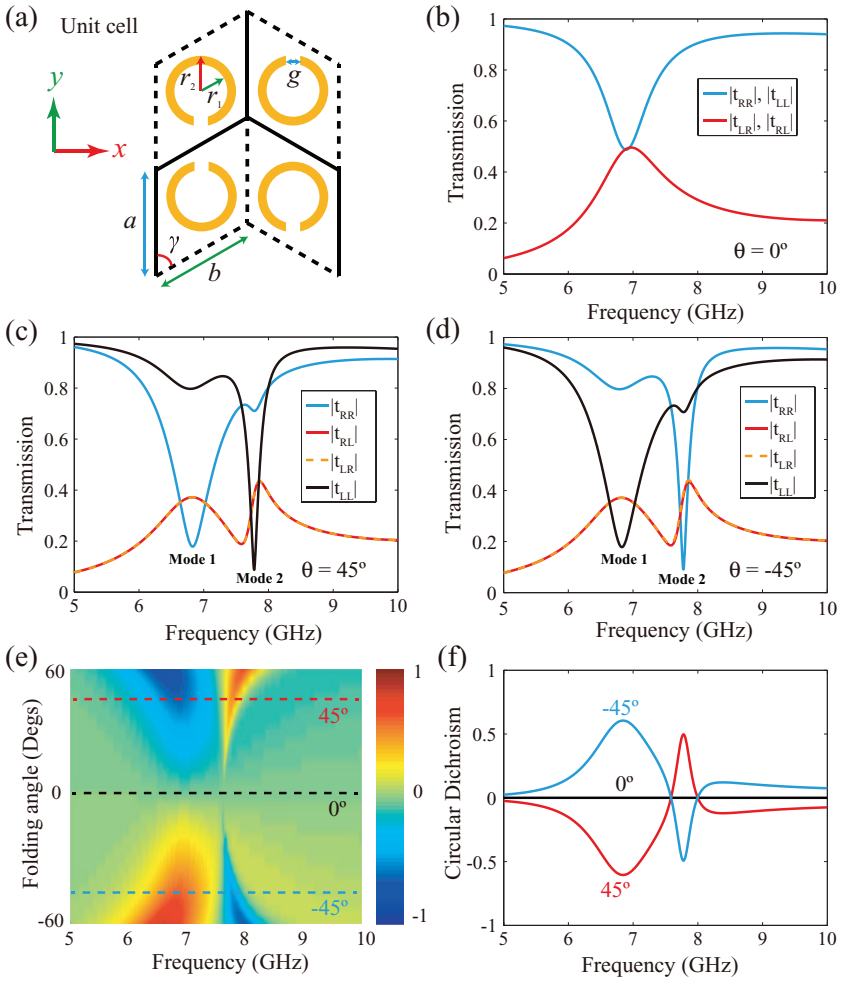

Figure 2. Dimensions and chiral responses of the Miura-ori metamaterial. a) Dimensions of the unit cell of Miura-ori metamaterial. Simulated transmission spectra of b) the unfolded achiral metasurface, c) enantiomer A and d) enantiomer B under the illumination of circularly polarized waves propagating along the *z*-axis. e) The CD spectra and f) selected CD curves of the Miura-ori metamaterial for different folding angles.

Full wave simulations have been performed to investigate the electromagnetic responses of the Miura-ori metamaterial under different folding states. In the simulations, the geometric modeling is feasible for a planar dielectric substrate, yet it becomes considerably complicated when the substrate is folded to 3D Miura-ori shapes. To simplify the simulation process for folded structures, here we neglect the dielectric substrate and the split-ring resonators are assumed to suspend in free space. A dielectric substrate with ultrathin thickness only changes the effective capacity in the gap, and therefore slightly shifts the resonant frequency of a split-ring resonator. The underlying physics of Miura-ori chiral metamaterials will not be affected (Supporting Information). In the unfolded state, the Miura-ori metasurface shows a resonant frequency at 6.9 GHz where the co-polarization transmission coefficient reaches its minimum (Figure 2b). This feature is owing to the strong electric resonances of the split-rings along the *x*-direction and thereby *x*-polarized waves are completely reflected. In its folded state of $\theta = 45°$, the Miura-ori metamaterial exhibits chiral-selective responses around this resonant frequency (labeled as mode 1), and an additional resonant mode (labeled as mode 2) emerges at a higher frequency of 7.78 GHz (Figure 2c). It is notable that mode 1 is a right-handed resonant mode in which most of the LCP wave is transmitted ($t_{LL} = 0.8$) while the opposite polarization is largely blocked ($t_{RR} = 0.18$). In contrast, the chiral response is reversed for mode 2 for which the structure is more transparent under RCP incidence ($t_{LL} = 0.1$, $t_{RR} = 0.7$). The switching between two enantiomers can be obtained by folding the Miura-ori in the opposite direction, resulting in the completely reversed chiroptical responses (Figure 2d). Nevertheless, the off-diagonal elements of the Jones matrices are preserved during the folding procedures, which represent the ability of polarization conversion between the two spin states. This feature originates from its additional rotational symmetry with respect to the *x*-axis. For a reciprocal medium with this type of symmetry, the structure is identical from both sides and thereby the off-diagonal elements have equal magnitude yet opposite signs.[44]

To better understand the performance of the Miura-ori metamaterial, we further investigate its CD spectra for different folding angles (Figure 2e). Here, the CD is calculated by $CD = |t_{RR}|^2 - |t_{LL}|^2$, which describes the discrepancy of two circularly polarized waves in transmission. The upper region ($\theta > 0$) of Figure 2e represents the performance of enantiomer A and the lower region ($\theta < 0$) is the counterpart for enantiomer B. It is clearly demonstrated that the chiroptical effects of these two enantiomers are complementary to each other and the chiral responses are significantly enhanced as the folding angle increases. In addition, the first resonance mode undergoes a redshift while the second resonance mode blueshifts, because the change of the periodicity influences the interactions between neighboring resonators. Specifically, the CD curves for three particular states ($\theta = 0°$, 45°, –45°) are separately plotted in Figure 2f. The CD of enantiomer A with a folding angle $\theta = 45°$ can reach as high as 0.6 at the first resonant mode and –0.5 at the second resonant mode.

To demonstrate the proposed reconfigurable metamaterials, Miura-ori patterns have been fabricated and characterized in the microwave region (**Figure 3**a). Copper split-ring resonators (thickness 0.035 mm) are periodically printed on a Halogen-free frame-resistant type polyimide film (thickness 0.05 mm) with a permittivity of 3.5. Since the Miura-ori pattern has a negative Poisson's ratio, the periodicity of the unit cell, both in the *x*- and *y*-directions, simultaneously decreases as the folding angle increases. Interestingly, the structure compresses much faster in the *x*-direction and ultimately achieves almost zero periodicity at its fully folded state. Such ultra-large dynamical

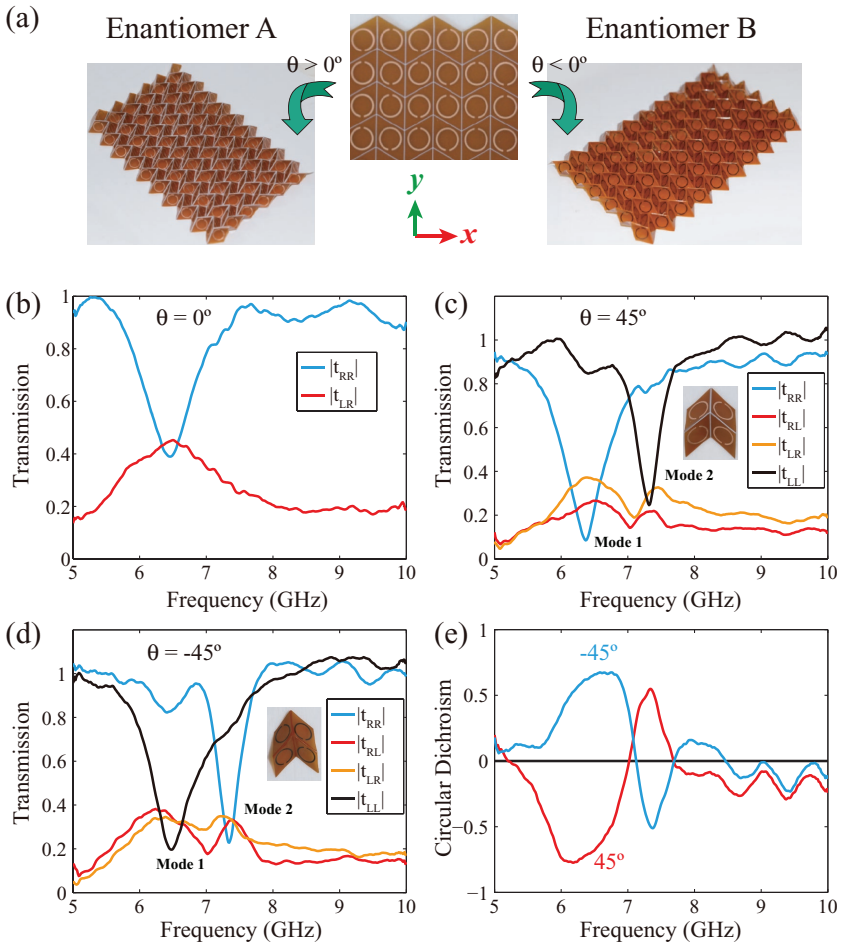

Figure 3. Experimental demonstration of the reconfigurable Miura-ori metamaterials. a) Photographs of the fabricated 2D Miura-ori pattern (middle panel) and the two enantiomers after positive (left panel) and negative (right panel) folding processes. b) Measured transmission spectra of an unfolded Miura-ori pattern with a dielectric substrate. c,d) Measured transmission spectra for enantiomer A and B with the folding angles of +45° and −45°, respectively. The insets show the photographs of single Miura-ori units. e) CD spectra of the two enantiomers calculated from (c) and (d).

range is one of the most attractive characteristics of the origami patterns that can hardly be implemented in other reconfigurable technologies.

The chiroptical response and chirality switching of the Miura-ori metamaterial have been experimentally investigated through measurements using a vector network analyzer. The details are described in the Experimental Section. Figure 3b shows the measured transmission spectra of the planar Miura-ori structure before folding. Compared with the planar metasurface suspended in free space (Figure 2b), the resonant frequency of the fabricated sample undergoes a small redshift (from 6.9 to 6.5 GHz) because of the permittivity of the substrate, which increases the capacitance induced at the gap of each split-ring resonator (see additional discussions on the influence of the substrate in the Supporting Information). When the metasurface is deformed to folded geometries, the mirror symmetry of the structure is broken and thereafter the chiroptical response emerges. This is demonstrated by the transmission dips at the two resonant frequencies in the transmission spectra (Figure 3c,d). At the first resonant frequency around 6.4 GHz, enantiomer A behaves as a right-handed metamaterial that blocks most of the RCP waves while enantiomer B, in contrast, is more transparent for this spin state. The situation is reversed for the second resonant mode at about 7.3 GHz, in which enantiomers A and B reverse their handedness of chirality. The measured CD spectra are plotted in Figure 3e, which clearly demonstrates the performance of chirality switching at the two resonant frequencies as predicted by the preceding simulations (Figure 2f). In our experiment, a flexible material is selected as the substrate to reduce the difficulty in folding process. Therefore, the facets are not strictly rigid and the deformations could be slightly discrepant among different folded Miura-ori units. The inhomogeneous deformation might result in unexpected resonant modes and some oscillations in the experimental spectra. The measurement error in phase and the noise from the environment could also cause the mismatch between the simulation and experimental results at high frequencies. The chiroptical response of the Miura-ori metamaterials for other folding angles and vertex angles can be found in the Supporting Information.

The microscopic origin of the chiroptical response in our Miura-ori metamaterials can be understood by the dipolar analysis (**Figure 4**). Split-ring resonators produce effective electric and magnetic dipoles at the resonance. The specific combination of the two dipoles, that is, parallel or antiparallel orientations with comparable magnitude, can induce strong chiral responses similar to natural chiral molecules.[45,46] To clarify the behavior of each split-ring resonator, we label the four parallelograms of a Miura-ori unit with particular numbers (Figure 4a). For the unfolded Miura-ori pattern, the normal vectors of the facets are given by $\hat{n}_i = \hat{z}$ (i = 1, 2, 3, 4). The surface current distribution at the resonant frequency of 6.9 GHz is plotted in Figure 4b, when the electric field of the incident wave is polarized along the x-axis. The induced electric and magnetic dipoles of the four split-ring resonators can be expressed as $\overline{p}_i = p_i\hat{x}$ and $\overline{m}_i = m_i\hat{z}$, respectively. The two dipole moments of each resonator are orthogonal to each other and oscillate with a frequency-dependent phase difference. Specifically, the electric dipoles of the four resonators have identical orientations, while the direction of the magnetic dipole is highly dependent on the orientation of each split-ring resonator. This corresponds to the anti-symmetric modes.[47] The out-of-plane magnetic dipoles do not radiate electromagnetic waves in the z-direction and hence no chiroptical response occurs for the unfolded structure, consistent with the conclusion from the symmetry consideration.

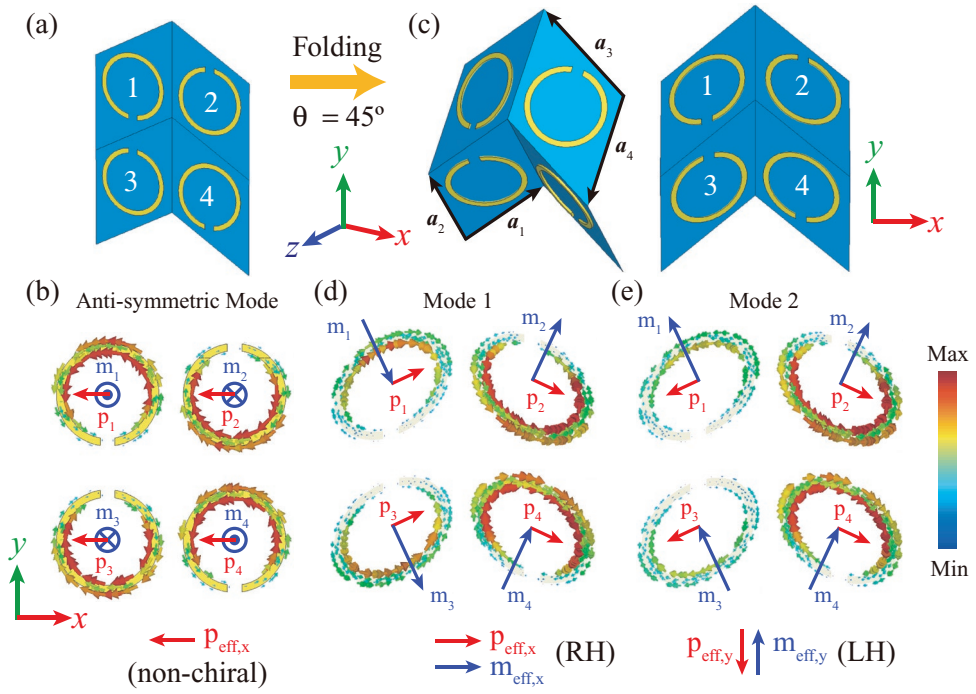

Figure 4. Simulated surface current distributions unraveling the underlying mechanism of the chiroptical response of the Miura-ori metamaterials. The orientation of a) the four split-ring resonators and b) their surface current distributions at the resonant frequency of 6.9 GHz. Four resonators all work on the asymmetric modes with in-plane electric dipoles and out-of-plane magnetic dipoles. c) Perspective and front views of a unit cell of enantiomer A. The surface current distributions for d) the first and e) second resonant modes. The induced electric and magnetic dipoles have parallel components at mode 1 but anti-parallel components at mode 2, leading to the opposite handedness of the Miura-ori metamaterial at the two resonant frequencies.

The situations are completely distinct for the folded patterns. We take enantiomer A as an example with a folding angle of $\theta = 45°$. After folding, the normal vectors of the facets are no longer along the same direction. Instead, they are given by $\overline{n}_1 = -\frac{\overline{a}_1 \times \overline{a}_4}{a^2}$, $\overline{n}_2 = \frac{\overline{a}_3 \times \overline{a}_4}{a^2}$, $\overline{n}_3 = \frac{\overline{a}_1 \times \overline{a}_2}{a^2}$, and $\overline{n}_4 = -\frac{\overline{a}_3 \times \overline{a}_2}{a^2}$, respectively, where $\overline{a}_i$ is the ith edge vector of the parallelogram as illustrated in Figure 4c. At the first resonant frequency (mode 1), the incident electric field excites the anti-symmetric modes of the split-rings and the induced electric dipoles are given by $\overline{p}_1 = p_1 \frac{\overline{n}_1 \times \overline{a}_4}{a}$, $\overline{p}_2 = p_2 \frac{\overline{n}_2 \times \overline{a}_4}{a}$, $\overline{p}_3 = -p_3 \frac{\overline{n}_3 \times \overline{a}_2}{a}$, and $\overline{p}_4 = -p_4 \frac{\overline{n}_4 \times \overline{a}_2}{a}$, as shown in Figure 4d. The induced magnetic dipoles, in contrast, are expressed as $\overline{m}_i = m_i \overline{n}_i$. The total effective electric and magnetic dipoles are then obtained $\overline{p}_{\text{eff}} = \sum \overline{p}_i = p_{\text{eff},x}\,\hat{x} + p_{\text{eff},y}\,\hat{y} + p_{\text{eff},z}\,\hat{z}$ and $\overline{m}_{\text{eff}} = \sum \overline{m}_i = m_{\text{eff},x}\,\hat{x} + m_{\text{eff},y}\,\hat{y} + m_{\text{eff},z}\,\hat{z}$, respectively. It is noticeable that at the first resonant frequency the in-plane components of both the effective electric and magnetic dipoles are mainly oriented in the x-direction, especially when the magnitudes of dipoles are comparable in the four split-ring resonators. The x components of the effective electric and magnetic dipoles are parallel with each other and this fact contributes to the strong right-handed chiral response, making the Miura-ori metamaterial less transparent for RCP waves. In addition, the facets of the Miura-ori patterns are no longer parallel with the incident magnetic field (H_y). Therefore, the magnetic responses of the split-ring resonators rise up and the strengths of the electric and magnetic dipoles are not exactly equal for each split-ring resonator. In particular, the normal component of the incident magnetic field is parallel to the magnetic dipoles in the second and the fourth split-ring resonators, and thus results in enhanced resonant responses. At the second resonant frequency (mode 2), the magnetic responses induced from the incident magnetic field are dominant and the in-plane effective dipoles are mainly oriented in the y direction (Figure 4e). Interestingly, the y components of the effective electric and magnetic dipoles are now anti-parallel with each other and therefore the Miura-ori metamaterial shows a left-handed chiral response. Similarly, the strengths of induced dipoles are not identical for different split-ring resonators owing to the coupling of electric and magnetic responses. The animations of the surface current for modes 1 and 2 (corresponding to Figure 4d and 4e, respectively) can be found in the uploaded videos, which offer a good visualization for the modes and induced dipoles.

An important feature of the Miura-ori metamaterial is its relative density, which can be substantially reduced by folding. This quantity is given by the ratio between the volumes before and after folding procedure[34]

$$\rho_{\text{rel}} = t \cdot \frac{ab \sin\gamma}{HSL} \tag{1}$$

where t is the thickness of the metamaterial sheet, $H = a \cdot \sin\gamma |\sin\theta|$ is the height of the vertex after folding, and $S = b \cdot \frac{\cos\theta \tan\gamma}{\sqrt{1+\cos^2\theta \tan^2\gamma}}$ and $L = a \cdot \sqrt{1-\sin^2\theta \sin^2\gamma}$ are the center distances between neighboring split-ring resonators

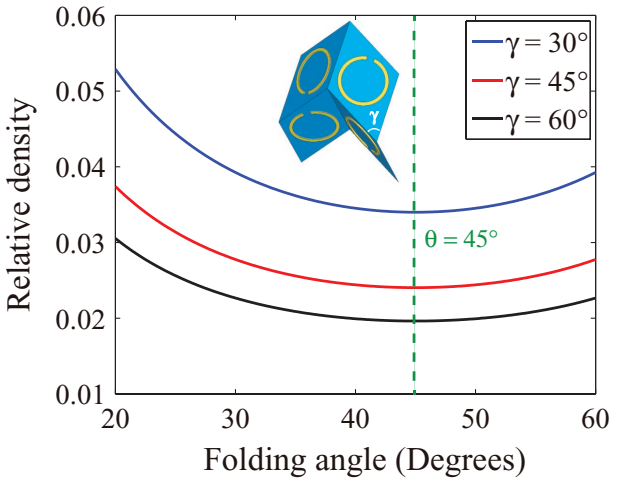

Figure 5. Dependence of the relative density of the Miura-ori metamaterial on the folding angle θ. The relative density of the fabricated sample reaches its minimum when the vertex angle $\gamma = 60°$, which is 98% lighter than the planar metasurface before folding.

in the *x*- and *y*-directions, respectively. The relative density of the Miura-ori metamaterial is plotted in **Figure 5**. The outer volume of the Miura-ori metamaterial is greatly increased during folding and therefore the relative density is dramatically reduced by several orders of magnitude. In particular, when the folding angle is 45° (or −45°), the relative density of the fabricated sample ($\gamma = 60°$) reaches its minimum $\rho_{\text{rel}}^{\min} = 0.0196$, indicating that the 3D Miura-ori metamaterial can be 98% lighter than the planar metasurface before folding. In addition, increasing the vertex angle γ of the parallelogram can also efficiently reduce the relative density (Supporting Information). This attractive feature is extremely useful to design lightweight and deployable metadevices for future applications.

In summary, we have proposed an origami approach to transform 2D metasurfaces to 3D metamaterials, which gives rise to folding-induced chirality in a continuously alterable manner. The deformation of the Miura-ori unit along the third dimension induces net electric and magnetic dipoles of split-ring resonators parallel or anti-parallel to each other, leading to the strong chiral responses. The strong chiral resonance results in circular dichroism as large as 0.6 when the folding angle is 45°. The handedness of the Miura-ori chiral metamaterial is switchable by reversing the folding direction. Furthermore, the Miura-ori pattern of a rigid sheet has only one degree of freedom described by the folding angle, indicating that this metamaterial can be transformed into any desired shape and still preserves its folding motion. Importantly, the relative density of the Miura-ori metamaterial can be dramatically reduced during folding process and reaches its minimum of only 2% of that of a planar unfolded metasurface. In addition, the structure stiffness of this origami pattern can be greatly improved by either stacking individual Miura-ori sheets together or assembling origami into coupled tubes.[34,39] These prominent features of Miura-ori patterns provide a promising methodology to design lightweight, deployable, and portable metadevices that enable novel electromagnetic and mechanic functionalities simultaneously. Last but not least, due to the scaling properties of Maxwell's equations, the design principle proposed here is scale-independent and can be easily extended to terahertz, infrared, and even optical frequencies. With the ongoing development of the micromanufacturing techniques, such as shape memory alloys,[48] 4D printing,[49,50] and self-folding origami,[51] we expect that our work would open new avenues for creating shape-changing and switchable electromagnetic components for various applications in future optical engineering.

Experimental Section

Simulations: Full-wave electromagnetic simulations were performed using the commercial software of CST Microwave Studio 2014. In all simulations, unit cell boundaries were adopted along the *x*- and *y*-axes while open boundaries were defined in the *z*-direction. To simplify the simulation process, the folded Miura-ori patterns were considered in free space and the influence from the substrate that only slightly shifted the resonant frequency (see Figure 3b and the corresponding discussion) was ignored. Copper with a conductivity of 5.8×10^7 S m^{-1} was chosen as the metallic material to construct the split-ring resonators.

Microwave Measurement: The electromagnetic responses of Miura-ori metamaterials were performed in anechoic chamber using microwave broadband horn antennas and a vector network analyzer. To obtain the transmission coefficients of circularly polarized light, four linear co-polarization and cross-polarization transmission coefficients, i.e., t_{xx}, t_{yx}, t_{xy}, and t_{yy}, were measured. The transmission Jones matrix for circular polarization was then obtained from the following equation

$$\begin{pmatrix} t_{RR} & t_{LR} \\ t_{RL} & t_{LL} \end{pmatrix} = \frac{1}{2}\begin{pmatrix} t_{xx} + t_{yy} + i(t_{xy} - t_{yx}) & t_{xx} - t_{yy} - i(t_{xy} + t_{yx}) \\ t_{xx} - t_{yy} + i(t_{xy} + t_{yx}) & t_{xx} + t_{yy} - i(t_{xy} - t_{yx}) \end{pmatrix} \quad (2)$$

where the first and second subscripts represent the incident and transmitted wave, *L* and *R* correspond to the LCP and RCP waves, and *x* and *y* represent the two linearly polarized waves with the electric fields polarized along two orthogonal directions.

Supporting Information

Supporting Information is available from the Wiley Online Library or from the author.

Acknowledgements

Y.L. acknowledges the support from the Office of Naval Research (N00014-16-1-2049). H.C. acknowledges the financial support from the National Natural Science Foundation of China under Grant Nos. 61625502, 61574127, and 61601408, the ZJNSF under Grant No. LY17F010008, the Postdoctoral Science Foundation of China under Grant No. 2015M581930, the Top-Notch Young Talents Program of China, and the Innovation Joint Research Center for Cyber-Physical-Society System. Work at Ames Laboratory was partially supported by the U.S. Department of Energy, Office of Basic Energy Science, Division of Materials Sciences and Engineering (Ames Laboratory is operated for the U.S. Department of Energy by Iowa State University under Contract No. DE-AC02-07CH11358). The European Research Council under ERC Advanced Grant No. 320081 (PHOTOMETA) supported work at FORTH.

Conflict of Interest

The authors declare no conflict of interest.

Keywords

metamaterials, origami, reconfigurable materials

Received: January 20, 2017
Revised: March 16, 2017
Published online: May 8, 2017

[1] Y. Liu, X. Zhang, *Chem. Soc. Rev.* **2011**, *40*, 2494.
[2] N. Meinzer, W. L. Barnes, I. R. Hooper, *Nat. Photonics* **2014**, *8*, 889.
[3] R. A. Shelby, D. R. Smith, S. Schultz, *Science* **2001**, *292*, 77.
[4] V. M. Shalaev, *Nat. Photonics* **2007**, *1*, 41.
[5] J. K. Gansel, M. Thiel, M. S. Rill, M. Decker, K. Bade, V. Saile, G. von Freymann, S. Linden, M. Wegener, *Science* **2009**, *325*, 1513.
[6] N. Fang, H. Lee, C. Sun, X. Zhang, *Science* **2005**, *308*, 534.
[7] J. B. Pendry, D. Schurig, D. R. Smith, *Science* **2006**, *312*, 1780.
[8] A. Kurs, A. Karalis, R. Moffatt, J. D. Joannopoulos, P. Fisher, M. Soljačić, *Science* **2007**, *317*, 83.
[9] N. Yu, P. Genevet, M. A. Kats, F. Aieta, J.-P. Tetienne, F. Capasso, Z. Gaburro, *Science* **2011**, *334*, 333.
[10] X. Chen, L. Huang, H. Mühlenbernd, G. Li, B. Bai, Q. Tan, G. Jin, C.-W. Qiu, S. Zhang, T. Zentgraf, *Nat. Commun.* **2012**, *3*, 1198.
[11] N. Shitrit, I. Yulevich, E. Maguid, D. Ozeri, D. Veksler, V. Kleiner, E. Hasman, *Science* **2013**, *340*, 724.
[12] M. Khorasaninejad, W. T. Chen, R. C. Devlin, J. Oh, A. Y. Zhu, F. Capasso, *Science* **2016**, *352*, 1190.
[13] N. Yu, F. Capasso, *Nat. Mater.* **2014**, *13*, 139.
[14] A. V. Kildishev, A. Boltasseva, V. M. Shalaev, *Science* **2013**, *339*, 1232009.
[15] N. I. Zheludev, Y. S. Kivshar, *Nat. Mater.* **2012**, *11*, 917.
[16] J.-Y. Ou, E. Plum, L. Jiang, N. I. Zheludev, *Nano Lett.* **2011**, *11*, 2142.
[17] H. Tao, A. Strikwerda, K. Fan, W. Padilla, X. Zhang, R. Averitt, *Phys. Rev. Lett.* **2009**, *103*, 147401.
[18] I. M. Pryce, K. Aydin, Y. A. Kelaita, R. M. Briggs, H. A. Atwater, *Nano Lett.* **2010**, *10*, 4222.
[19] J.-Y. Ou, E. Plum, J. Zhang, N. I. Zheludev, *Nat. Nanotechnol.* **2013**, *8*, 252.
[20] M. Lapine, I. V. Shadrivov, D. A. Powell, Y. S. Kivshar, *Nat. Mater.* **2012**, *11*, 30.
[21] J. Valente, E. Plum, I. J. Youngs, N. I. Zheludev, *Adv. Mater.* **2016**, *28*, 5176.
[22] T. Kan, A. Isozaki, N. Kanda, N. Nemoto, K. Konishi, H. Takahashi, M. Kuwata-Gonokami, K. Matsumoto, I. Shimoyama, *Nat. Commun.* **2015**, *6*, 8422.
[23] Q. Wang, E. T. Rogers, B. Gholipour, C.-M. Wang, G. Yuan, J. Teng, N. I. Zheludev, *Nat. Photonics* **2016**, *10*, 60.
[24] X. Yin, M. Schäferling, A.-K. U. Michel, A. Tittl, M. Wuttig, T. Taubner, H. Giessen, *Nano Lett.* **2015**, *15*, 4255.
[25] W. Forbes, *Psyche* **1924**, *31*, 254.
[26] H. Kobayashi, B. Kresling, J. F. Vincent, *Proc. R. Soc. London. B* **1998**, *265*, 147.
[27] M. B. Amar, F. Jia, *Proc. Natl. Acad. Sci. USA* **2013**, *110*, 10525.
[28] A. E. Shyer, T. Tallinen, N. L. Nerurkar, Z. Wei, E. S. Gil, D. L. Kaplan, C. J. Tabin, L. Mahadevan, *Science* **2013**, *342*, 212.
[29] Z. You, *Science* **2014**, *345*, 623.
[30] Y. Chen, R. Peng, Z. You, *Science* **2015**, *349*, 396.
[31] S. A. Zirbel, R. J. Lang, M. W. Thomson, D. A. Sigel, P. E. Walkemeyer, B. P. Trease, S. P. Magleby, L. L. Howell, *J. Mech. Des.* **2013**, *135*, 111005.
[32] Z. Song, T. Ma, R. Tang, Q. Cheng, X. Wang, D. Krishnaraju, R. Panat, C. K. Chan, H. Yu, H. Jiang, *Nat. Commun.* **2014**, *5*, 3140.
[33] S. Felton, M. Tolley, E. Demaine, D. Rus, R. Wood, *Science* **2014**, *345*, 644.
[34] M. Schenk, S. D. Guest, *Proc. Natl. Acad. Sci. USA* **2013**, *110*, 3276.
[35] Z. Y. Wei, Z. V. Guo, L. Dudte, H. Y. Liang, L. Mahadevan, *Phys. Rev. Lett.* **2013**, *110*, 215501.
[36] J. L. Silverberg, A. A. Evans, L. McLeod, R. C. Hayward, T. Hull, C. D. Santangelo, I. Cohen, *Science* **2014**, *345*, 647.
[37] S. Waitukaitis, R. Menaut, B. G.-g. Chen, M. van Hecke, *Phys. Rev. Lett.* **2015**, *114*, 055503.
[38] H. Yasuda, J. Yang, *Phys. Rev. Lett.* **2015**, *114*, 185502.
[39] E. T. Filipov, T. Tachi, G. H. Paulino, *Proc. Natl. Acad. Sci. USA* **2015**, *112*, 12321.
[40] J. B. Pendry, A. J. Holden, D. J. Robbins, W. J. Stewart, *IEEE Trans. Microwave Theory Tech.* **1999**, *47*, 2075.
[41] J. D. Baena, J. Bonache, F. Martin, R. M. Sillero, F. Falcone, T. Lopetegi, M. A. G. Laso, J. Garcia-Garcia, I. Gil, M. F. Portillo, M. Sorolla, *IEEE Trans. Microwave Theory Tech.* **2005**, *53*, 1451.
[42] E. Plum, V. Fedotov, N. Zheludev, *Appl. Phys. Lett.* **2008**, *93*, 191911.
[43] E. Plum, X.-X. Liu, V. Fedotov, Y. Chen, D. Tsai, N. Zheludev, *Phys. Rev. Lett.* **2009**, *102*, 113902.
[44] C. Menzel, C. Rockstuhl, F. Lederer, *Phys. Rev. A* **2010**, *82*, 053811.
[45] H. Alaeian, J. A. Dionne, *Phys. Rev. B* **2015**, *91*, 245108.
[46] S. Yoo, Q.-H. Park, *Phys. Rev. Lett.* **2015**, *114*, 203003.
[47] L. X. Liu, X. Q. Zhang, M. Kenney, X. Q. Su, N. N. Xu, C. M. Ouyang, Y. L. Shi, J. G. Han, W. L. Zhang, S. Zhang, *Adv. Mater.* **2014**, *26*, 5031.
[48] D. Ratna, J. Karger-Kocsis, *J. Mater. Sci.* **2008**, *43*, 254.
[49] Q. Ge, H. J. Qi, M. L. Dunn, *Appl. Phys. Lett.* **2013**, *103*, 131901.
[50] S. Tibbits, *Archit. Des.* **2014**, *84*, 116.
[51] J. H. Na, A. A. Evans, J. Bae, M. C. Chiappelli, C. D. Santangelo, R. J. Lang, T. C. Hull, R. C. Hayward, *Adv. Mater.* **2015**, *27*, 79.

